IEEE Photonics Journal
An IEEE Photonics Society Publication

Open Access

Self-Assembled Colloidal Photonic Crystal on the Fiber Optic Tip as a Sensing Probe

Volume 9, Number 2, April 2017

Pasquale Di Palma
Chiara Taddei
Anna Borriello
Giovanna De Luca
Michele Giordano
Agostino Iadicicco
Stefania Campopiano
Lucia Sansone

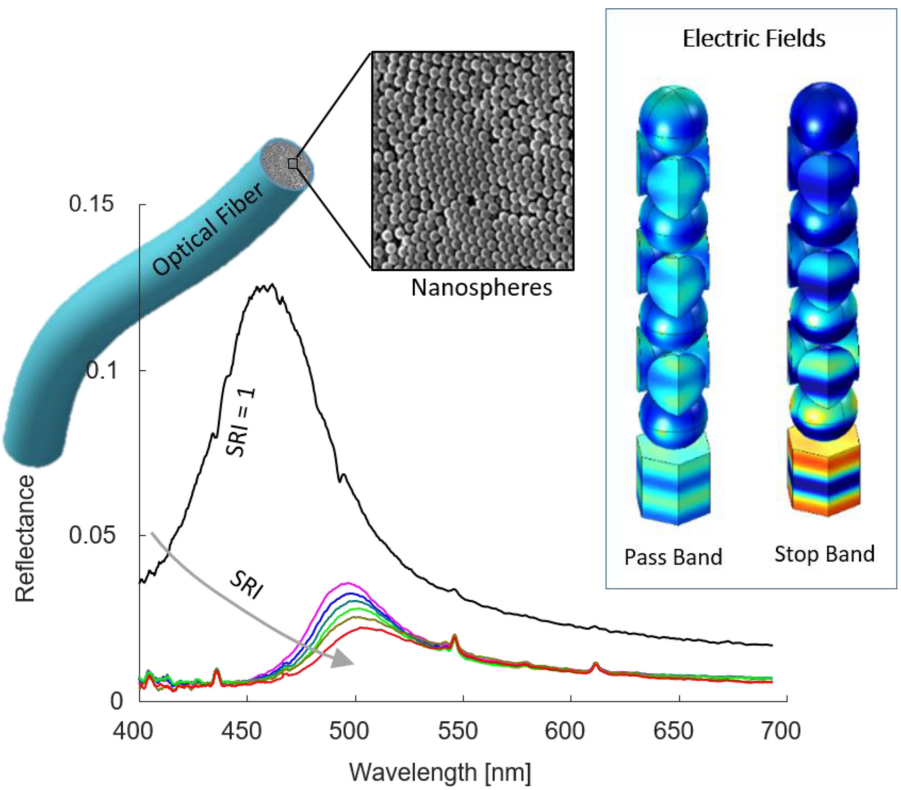

DOI: 10.1109/JPHOT.2017.2689075
1943-0655

IEEE photonics SOCIETY
IEEE

Self-Assembled Colloidal Photonic Crystal on the Fiber Optic Tip as a Sensing Probe

Pasquale Di Palma,[1] Chiara Taddei,[2,3,4] Anna Borriello,[5] Giovanna De Luca,[6,5] Michele Giordano,[5] Agostino Iadicicco,[1] Stefania Campopiano,[1] and Lucia Sansone[5]

[1]Department of Engineering, University of Naples Parthenope, Naples 80143, Italy
[2]Department of Chemical Materials and Production Engineering, University of Naples Federico II, Naples 80125, Italy
[3]Institut Charles Sadron, Strasbourg 67200, France
[4]Ecole de Chimie, Polymères et Matériaux, Université de Strasbourg, Strasbourg 67087, France
[5]Institute for Polymers, Composites and Biomaterials, National Research Council of Italy, Portici 80055, Italy
[6]Department of Chemical, Biological, Pharmaceutical and Environmental Sciences, University of Messina, Messina 98168, Italy

DOI:10.1109/JPHOT.2017.2689075

Manuscript received February 14, 2017; revised March 24, 2017; accepted March 24, 2017. Date of publication March 29, 2017; date of current version April 18, 2017. Corresponding authors: M. Giordano and A. Iadicicco (e-mail: gmichele@unina.it; iadicicco@uniparthenope.it).

Abstract: This paper presents an effective and efficient method to fabricate novel fiber optic sensing probes. The new, simple, and low cost approach is based on a 3-D photonic crystal dielectric structure directly deposited on the tip of a multimode optical fiber through the self-assembly of colloidal crystals (CCs) via a vertical deposition technique. Here, the CC is made of polystyrene nanospheres with 200 nm diameter, and the optical fiber is a UV–vis fiber with a core diameter of 200 μm. The obtained fiber probes exhibit a resonant peak at 480 nm and an amplitude enhancement of 3.7 with respect to the bare fiber; these results are highly repeatable. A numerical tool based on a finite element method analysis has been developed to study and analyze the 3-D subwavelength structures. Numerical results are in good agreement with the observed experimental spectra. Moreover, refractive index measurements have been carried out, revealing a sensitivity of up to 445 nm/RIU in the 1.33–1.36 values range. The achieved performances, which have been obtained by using very small active areas and an easy and reliable fabrication procedure, demonstrate the future perspectives of these fiber-optic probes for chemical and biological sensing applications.

Index Terms: Fiber optic sensor, photonic crystal, colloidal crystal, self assembly.

1. Introduction

Since their introduction in 1987 [1], [2], photonic crystals (PhCs) have been extensively studied as high effective sensors for environmental monitoring and chemical and biological detections. Photonic crystals are structures in which the dielectric constant (refractive index) has an artificial periodic variation in one, two or in all three orthogonal directions (1-D, 2-D, or 3-D) with a period close to the wavelength of the electromagnetic wave [3]–[5]. This periodicity affects the propagation

of electromagnetic waves in the material due to Bragg reflections on lattice planes. The result is a photonic bandgap (PBG) that is a band of frequencies where light propagation in the photonic crystal is forbidden.

Due to the PBG, photonic crystals offer unique ways to control and manipulate the light and represent one of the most popular class of photonic sensors that are generally employed for physical and chemical/biochemical sensing [6]–[9].

However, even though the theory of photonic crystals has been extensively studied over the years and many phenomena are predicted with photonic crystals in the visible and near-IR wavelength regions, the experimental realization of these crystal structures is still not easy and faces several fabrication difficulties [10]. The common approaches to make artificial periodic structures are based on the use of high-resolution and expensive micro-nano-machining techniques involving focused ion beam, electron beam lithography and more [11]–[13]. However, fabrication of 3-D photonic crystals is quite challenging as compared with 1-D or 2-D photonic structures.

On the contrary, spontaneous physical mechanisms could be used to overcome most of the fabrication limitations. In particular, the self-assembly CCs are a three-dimensional close-packed crystal of submicrometer spheres, formed via self-assembly of particles ranging in size from nanometers to micrometers into crystalline arrays [14]. It is dubbed bottom-up nanofabrication and permits self-assembly of constructs in parallel manner from nanoscale building blocks [15]. In the past two decades, self-assembly CCs received great attention in optoelectronics and photonics devices [15], [16]. The self-assembly of CCs can be achieved by gravity sedimentation, vertical deposition, electrophoresis, spin coating, crystallization in physically confined cells, and other methods. Compared to other methods, vertical deposition [17] is the most widely used and improved to form large scale colloidal crystals with controllable thickness and high quality. The ability to manipulate the self-assembly of colloidal particles, e.g., through the control of the temperature or pressure, or changing the nature of the employed solvents, has led to a better understanding of the underlying physical principles, as well as they have extended the application of this method to create functional architectures such as photonic waveguides, switches, optical filters, as well as chemical and biochemical sensors [18]. Among the materials used for colloidal crystals, the most widely spread are silica and polymers [19].

On the other hand, it is worth highlighting that optical fibers are a long established technology for light transport, but are increasingly being used for sensing purposes [20].The concepts behind the photonic bandgap have been also combined with fiber optics technology leading to hollow core photonic bandgap fibers where light is guided in the air core [21]–[25]. Furthermore, the challenge in exploiting the PBG sensing features in miniaturized optical fiber devices favorites the introduction of a large number of sensing configurations realized on the tip of the optical fiber. Indeed, the flat tip of an optical fiber is an inherently light-coupled platform for micro-and nanostructures and may act as a technological substrate for the realization of nanoscaled sensing devices [16],[1] [26]–[28]. Recently, the field of 'lab on a fiber' has emerged, giving rise to state-of-the-art fiber sensing applications that rely on the micro- and nanofabrication of devices at the tip of the fiber [29]–[31]. Many dedicated technological approaches have been developed to manufacture resonant structures on standard or specially designed fiber tips [14], [29], [32], [33]. In most cases, the resonant structures are combined with plasmonic effects in order to enhance the sensing features of the final devices [34]–[38]. In this framework, the most promising configuration appears to be based on hybrid metallo-dielectric nanostructures capable of localized surface plasmon resonance (LSPRs) and surface enhanced Raman scattering (SERS) [39], [40]. However, in most of the existing sensing probes involving nanostructures integrated with fiber tips the fabrication procedures demand expensive equipment [29], [41]. On the contrary, approaches based on the self-assembly of CCs could enable the fabrication of high performance probes with low-cost processes and high throughput. The challenge in exploiting CCs self-assembled on fiber tips arises from the difficulty of creating the CCs layers with high control on this unconventional surface [42], [43]. Haibin *et al.* [44] realized a fiber capillary structure which helps the self-assembly of polystyrene (PS) nanoparticles on the fiber optic tip, and they used this structure to measure the reflection index difference of two different solvents to develop a gas sensor. Cusano *et al.* [45] suggested a

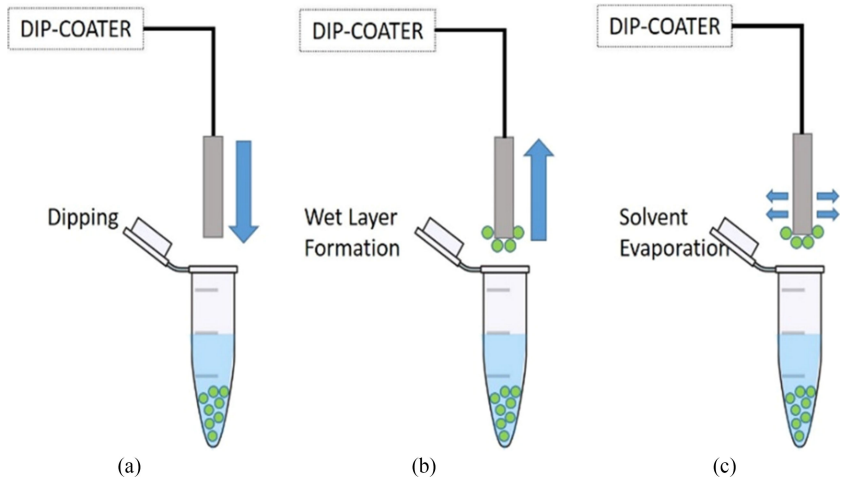

Fig. 1. Schematic diagram of the dip coating process. (a) Fiber tip is dipped at a constant speed into the colloidal solution. (b) Tip is extracted at a constant speed, and a wet nanoparticles layer is formed. (c) After solvent evaporation, a PS photonic crystal is formed right at the fiber tip.

fabrication route for self-assembling periodic patterns on optical fiber tips based (i) on the self-assembly of PS microspheres at the air/water interface and (ii) on the subsequent transfer of the monolayer colloidal crystal on the fiber tip. These steps have been followed by further treatments such as particle size reduction, metal coating and sphere removal, with the formation of different periodic structures at the fiber tip. The results obtained so far indicate that self-assembly affords a concrete opportunity to create ordered arrays of dielectric, metallic, and hybrid spheres or patterns with a submicron-scale feature size at low fabrication costs.

In this paper, we present the formation of a self-assembled colloidal photonic crystal onto the tip of an UV-VIS optical fiber, having a core diameter of 200 μm, through the vertical deposition of a colloidal solution of PS nanospheres with a 200 nm mean diameter.

The fabricated prototypes exhibit high finesse resonances in the reflected spectrum with high repeatability rate and with extremely appealing features, like cheapness, simplicity and sensitivity, for sensing applications in the chemical and biological fields. Moreover, the optical principle giving rise to high resonances in the reflected spectrum is discussed, supported by a wide numerical analysis and a comparison with the experimental data.

2. Results and Discussion

2.1. Fabrication and Morphological Characterization

2.1.1. Even More Details: Monodispersed polystyrene (PS) beads (aqueous dispersions, 10% w/ w) were purchased from Sigma Aldrich (Italy) and used as received. The particles used in this study have a diameter of 200 nm (from data sheet).

2.1.2. Particle Deposition: An UV-VIS multimode fiber optic, 200 μm core (Thorlabs, U.S.A.), was cut by using a high precision cleaver (Fujikura, Tokyo, Japan), and then vertically dip-coated in the PS nanoparticles suspension by means of an automated dip coater system (NIMA Technology Micro-Processor Interface IU4, Spain) at an immersion/extraction speed of 107 mm/ min (see Fig. 1). After the evaporation of solvent, an ordered PS pattern has been formed on the tip of the optical fiber. For the experiments reported in this paper only one dip was performed.

Fig. 2 shows scanning electron microscopy (SEM) micrographs of the fiber tip covered by the assembled PS beads at different magnifications, the periodic structure of the PS beads assembly being clearly evident.

2.1.3. Spectral Characterization: The PhC structures self-assembled on the fiber tip have been optically characterized in the visible range. Reflectance measurements have been carried out by

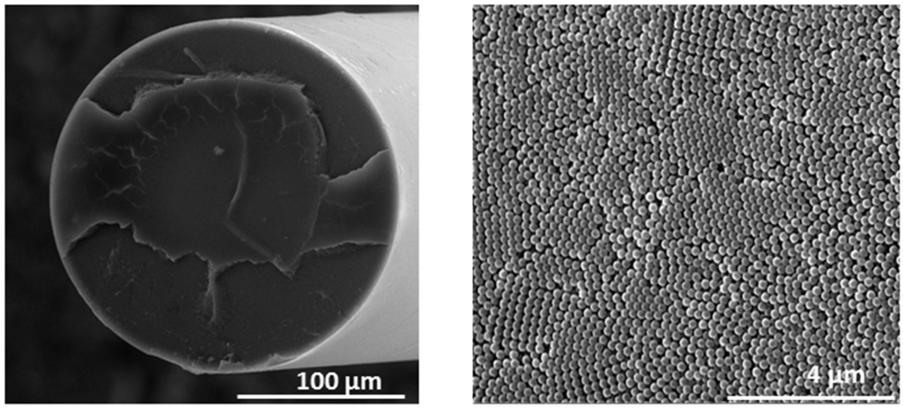

Fig. 2. SEM micrographs of periodic structures formed upon deposition of a PS photonic crystal on the optical fiber tip.

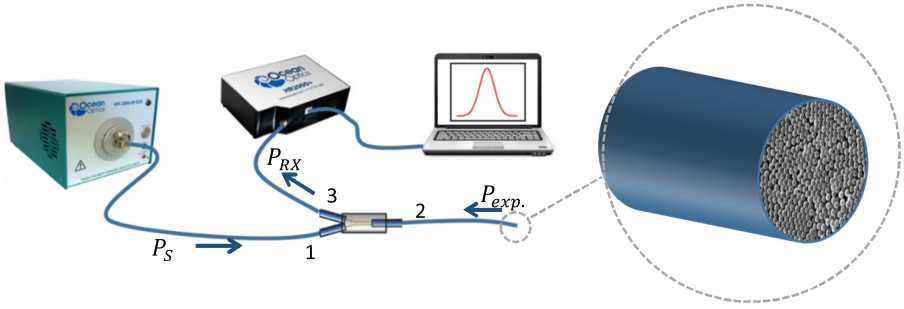

Fig. 3. Schematic representation of the setup for measuring the reflection spectra of the PS photonic crystal deposited on the fiber tip.

illuminating the fiber tip with a xenon optical source (OceanOptics HPX-2000 185–2000 nm) and redirecting the reflected light to an optical spectrum analyzer (OceanOptics, HR 2000+) by means of a lab-grade 3 dB fiber splitter. The optoelectronic setup is schematically plotted in Fig. 3.

The selected fibers (including the coupler) are characterized by a 200 μm core and 240 μm cladding.

Fig. 4 shows the reflectance spectrum of the PS nanoparticles layer deposited on the fiber tip, compared with the spectrum of the bare fiber and together with the results of the numerical simulations, the experimental spectrum having been normalized to the incident power. The reflectance spectrum of the bare fiber tip exhibits a quasi-constant value of about 3.4% in agreement with the expected amount of light reflected back from the fiber glass–air interface. As the PS nanospheres are deposited on the fiber tip, the experimental spectrum shows a peak with a reflectance maximum of about 12.5% centered at 458 nm with a 3 dB-bandwidth of 54 nm. Therefore, in comparison with the bare fiber (our reference), an enhancement of the reflected light intensity of about 3.7 is obtained at the wavelength of the peak maximum. Out of the observed band, the reflectance of the PhC structure formed by the PS nanospheres is almost comparable to that of the bare fiber, confirming that the wavelength-selective enhancement of the reflectance is due to a photonic bandgap caused by the periodic self-assembly of the PS nanospheres at the fiber tip.

2.2. Numerical Analysis

In order to better understand the experimental results, numerical simulations have been performed using the commercial software COMSOL Multiphysics (RF module) based on the FEM, this step being also useful to identify design criteria for the control of the spectral features. To this aim,

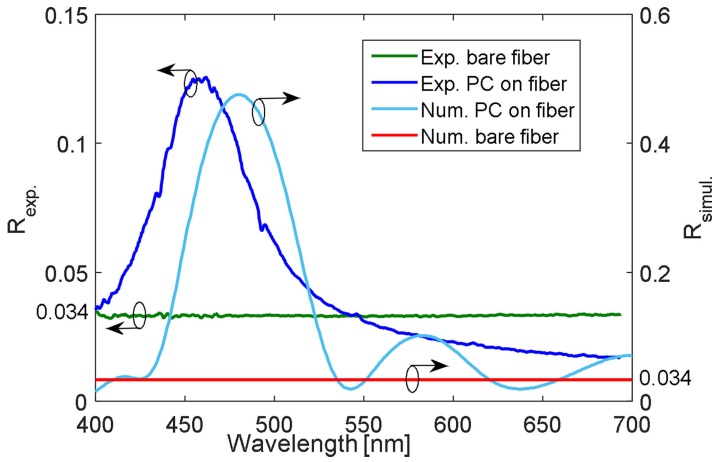

Fig. 4. Measured reflection spectra of bare fiber tip in air (green line) and PS assembled in air (blue line) compared to simulated bare fiber tip in air (red line) and PS assembled in air (azure line).

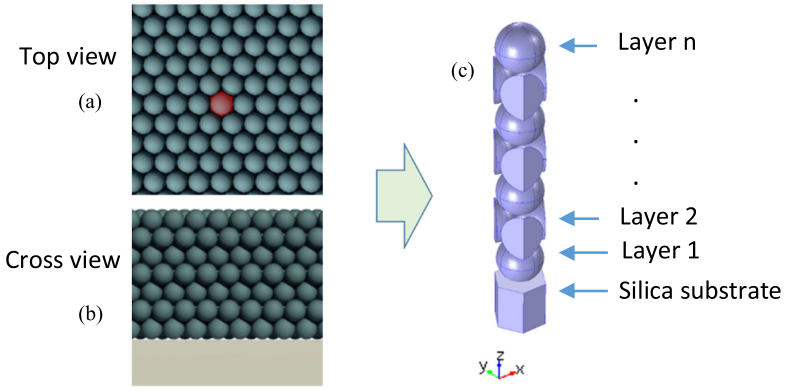

Fig. 5. Schematic illustration of the PC structure. (a) Top and (b) cross view of the simplified slab approach with the elementary cell highlighted in red. (c) Hexagonal unit cell.

polystyrene nanospheres of 200 nm diameter, which is in agreement with the nanoparticles nominal diameter value, were used for simulations.

In order to simplify the computation of the photonic crystals reflectance, the simulation does not take into account the finite size of the lattice (as the real one), the 3-D structure considered in this study being schematically represented in Fig. 5. It mainly consists of a silica glass substrate covered with a hexagonal close-packed (HCP) lattice of PS nanospheres, with a resulting filling factor $k_f = \frac{\pi}{3\sqrt{2}} = 0.7405$. Fig. 5(a) and (b) show schematic top and cross view of the 3-D colloidal crystal. When such a structure is illuminated with a plane wave orthogonal to the silica surface, the photonic bandgap will cause a reflected resonance peak, that will be associated with a trough in transmission. The resonance peak is a reflected wavelength interval where a constructive interference between the waves reflected at each interface occurs and depends on the optical and geometric features of the structure itself.

A common approach requires the calculation of the scattering parameters of a slab which can be simulated as the unit cell with periodic boundary conditions [46], [47]. The unit cell consists in a hexagonal silica glass base that inscribes a circumference with the same radius as the nanospheres one [see Fig. 5(c)]. The different layers of nanospheres alternatively consist in: (a) a single nanosphere and (b) in three wedges being one third of a nanospheres each. This arrangement arises from the nanoparticles organization typical of the HCP lattice. The refractive indices used for modeling the silica surface and the PS nanospheres in the investigated wavelength

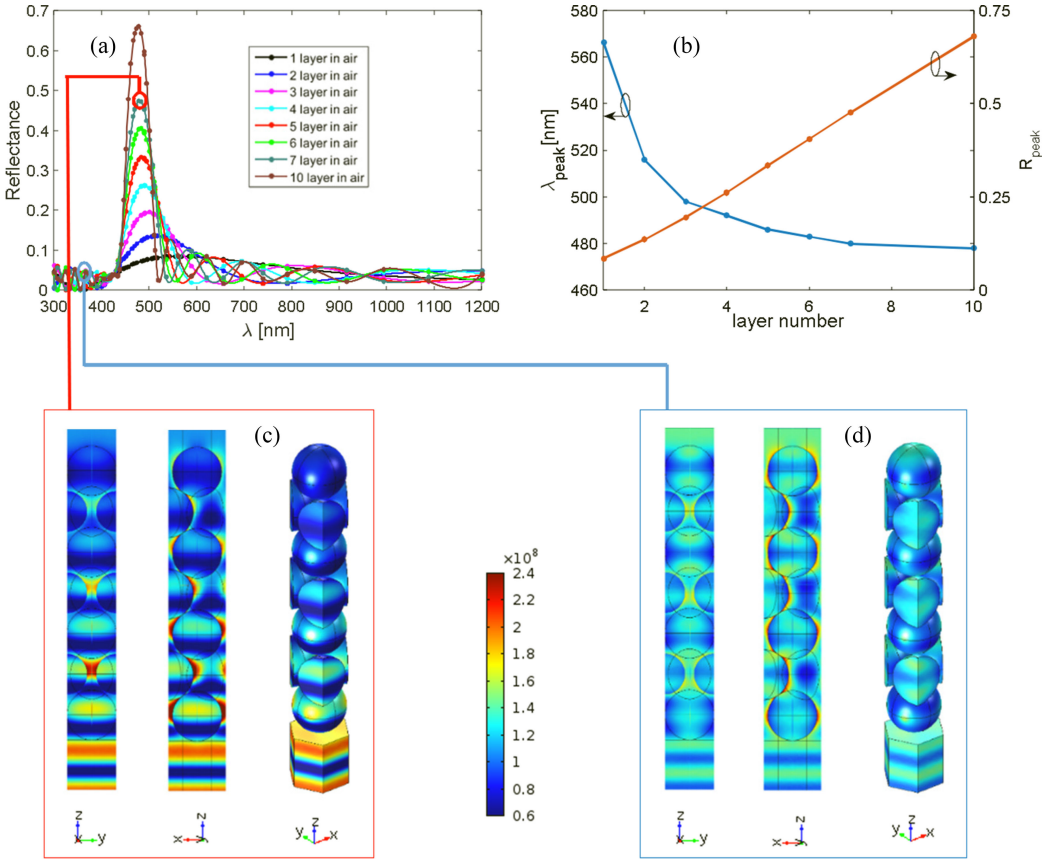

Fig. 6. (a) Simulated spectra as a function of the layers number in air. (b) Simulated resonance wavelength and intensity vs layers number. (c), (d) COMSOL images of the electric fields calculated on and off resonance, respectively.

domain is taken from [48] and [49], respectively, whereas the nanospheres diameter was d = 200 nm according to the datasheet. Afterwards small variations of these values will be considered in order to study the effects on the reflected spectrum.

The Perfectly Matched Layer (PML) absorbing boundary condition in the z direction over the nanospheres multilayer is used to simulate an infinite surrounding media over the PC structure. Periodic Floquet boundary condition are used to implement the periodicity in three directions, staggered by 120°, in the xy plane and placed two-by-two in the opposite walls.

It is worth noting that the number of layer plays an important role in determining the shape and amplitude of the resonance band in the reflected spectrum.

Fig. 6(a) shows the numerical reflectance spectra (normalized to the incident field power) for different numbers of layers. Clearly, the reflectance spectra show a positive peak in the reflected signal that strongly depends on the number of layers. The resonant wavelength exhibits a blue shift on increasing their number, whereas the peak amplitude strongly increases. As well, the reflected spectra show a band that narrows on increasing the layers number in reflected power, due to a photonic bandgap effect in the CC structure. Fig. 6(b) summarizes the dependence of the peak characteristics on the number of layers, calculated up to 10 layers. The resonant wavelength exhibits a blue shift with a convergent trend versus the layers number, practically reaching the asymptotic value after seven layers. A peak amplitude displays a different behavior, linearly increasing with the number of simulated layers. Given the trend, it is reasonable to believe that the maximum reflectance may reach the 100% with a higher number of layers, however this number had to be limited for computational reasons. The secondary lobes do not increase their amplitude, thus the

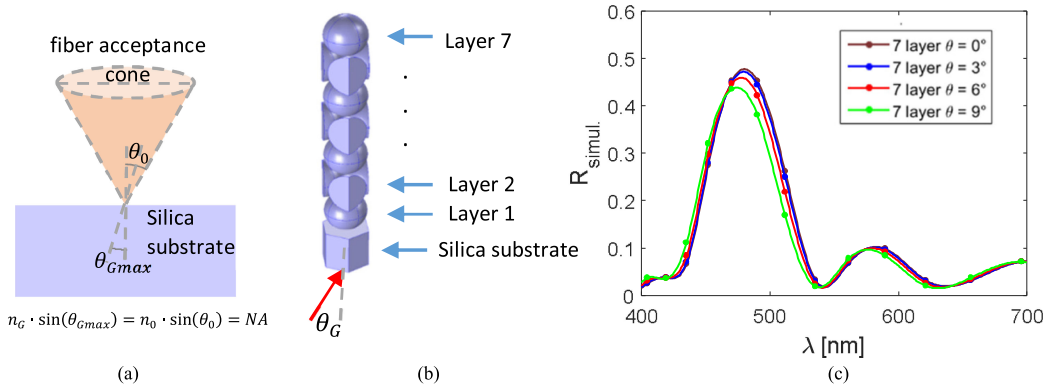

Fig. 7. (a) Schematic view of the maximum incident angle. (b) Unit cell with incident angle and (c) spectra simulated for different angles of incidence of the electromagnetic field.

ratio between the amplitudes of main and secondary lobes increases with the layers number. From these results, in order to limit the computational efforts, the number of layers is fixed to 7 in the following analysis.

Fig. 6(c) and (d) show the electrical field distribution at the resonance wavelength (479 nm) and away from it (345 nm), respectively, for a seven-layer structure. The 2-D graphs plot the field distribution in two perpendicular planes cutting the unit cell in the center and on the nanosphere surface, showing a significant field localization at the interfaces between the PS nanospheres and the surrounding dielectric (air in this case). This can be attributed to localized reflection-refraction of the electrical field due to the difference in the refractive indices (PS – air). Moreover, at the resonance wavelength [see Fig. 6(c)], the field amplitude decreases moving away from the silica substrate layer-by-layer whereas, out of the band [see Fig. 6(d)], the field amplitude on the nanospheres surfaces does not depend on the layer number.

Thus, the reflectivity enhancement at resonant wavelength confirms the predicted photonic bandgap properties of this structure and, consequently, all the advantages of using photonic crystals in sensing applications can be expected. Notably, despite the limited number of layers, all the investigated numerical cases display a reflectance peak amplitude which is significantly higher than the experimental one.

Fig. 4 compares the reflectance spectrum computed with 7 nanospheres layers with experimental data and it shows a good agreement between the experimental and numerical data, the main difference being found in the values of the peak amplitude values (12.5% and 47%, respectively). Moreover, the calculated peak exhibits a red shift of 20 nm as compared to the experimental one. These mismatches can be explained considering the unavoidable fabrication defects with respect to the ideal structure considered in the numerical analysis, as well as the tolerances in the nanospheres diameter and refractive index.

Evidently, the simulated planar structure differs from the real device (PhC on the fiber tip) in the lack of edges and in the incident excitation not taking into consideration the Gaussian-like wavelength distribution which results from the high number of incident modes with different angles at the silica-PhC interface. To assess this last approximation, numerical simulations have been carried out setting different angles of incidence (θ_G in Fig. 7), ranging from 0° to 9°, which is in agreement with the numerical aperture of the fiber optic.

The results [see Fig. 7(c)] show a negligible influence of the angle of incidence of the input beam on the reflectance spectrum, with a blue shift of the bandgap wavelength of 6.0 nm maximum on increasing the angle. This means that the numerical results, obtained with the simplest case of a plane wave orthogonally incident on the silica surface, are valid for predicting the experimental behavior and to be used as design tool, given a little approximation in the bandgap wavelength. Similar studies carried out to investigate the dependence of the reflectance spectra on the spheres diameters and refractive index show that (i) the increase in the spheres diameter induces a bandgap

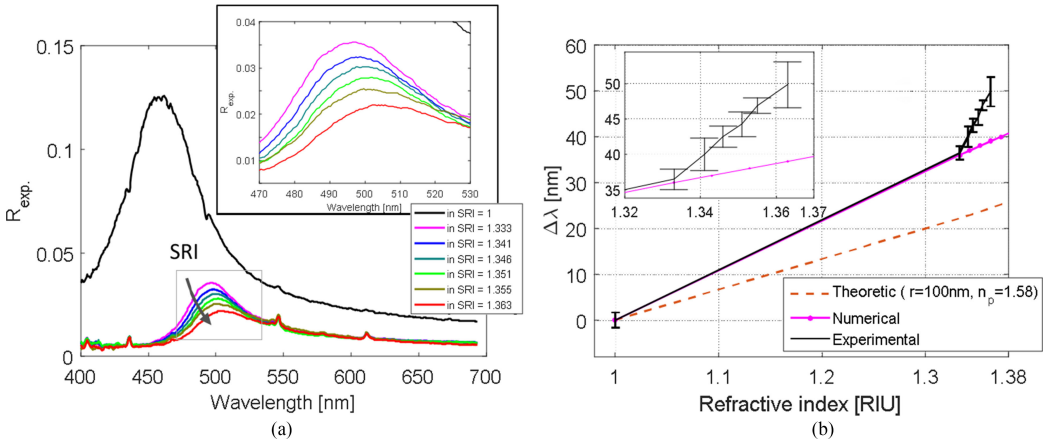

Fig. 8. (a) Experimental reflectance spectra of one sample as function of SRI. (inset) Zoomed view of the spectra for the 1.333–1.363 SRI range). (b) Wavelength shift of the bandgap peak vs SRI of numerical and experimental data, as well as the wavelength shift achieved by the theory of (1) [5]. (Inset) Zoomed view of the numerical and experimental data in the 1.333–1.363 SRI range.

wavelength shift with a rate of about 2.4 nm/nm with a negligible effect on the peak amplitude, and (ii) the changes in the spheres refractive index, i.e., in the PhC dielectric contrast, affect the bandgap wavelength of about 250 nm/RIU and the peak amplitude of 48%/RIU.

2.3. Refractive Index Sensitivity

Since the bandgap behavior of colloidal structures is strongly dependent on the contrast of dielectric periodicity, a significant sensitivity to the surrounding refractive index (SRI) is expected [5]. To assess the sensitivity of the proposed fiber probes to the SRI, reflectance spectra were measured while the optical fiber probes are immersed in different liquids with known refractive indices. To this aim, we used aqueous ethanol solutions with different concentrations where the refractive indices were measured by means of a Abbe refractometer with resolution of 10^{-4}. Moreover, several probes were selected in order to investigate the repeatability of the fabrication process with good results.

Fig. 8(a) reports the experimental spectra of a selected sample recorded for different SRI in the 1–1.363 range, the main effect being a significant red-shift of the bandgap wavelength combined with a modification of the reflectance amplitude and peak visibility.

The shifts of the experimental and numerical bandgap wavelength vs SRI are compared in Fig. 8(b), the experimental data having been recorded with different (more than 20) fiber probes fabricated in the same conditions and taking into consideration different surrounding media. These data are plotted as average values on all tests, indicating the standard deviations (values from 1.1 nm for SRI $=1.355$ to 3.2 nm for SRI $=1.363$) as error bars. Notably, when the external medium changes from air to water (SRI moving from 1 to 1.333) the experimental and numerical data are in very good agreement, exhibiting a wavelength shift of 36 nm in both cases (sensitivity: 108 nm/ RIU). Concerning the experimental data, further increases in the SRI induce a significant enhancement of the SRI sensitivity up to 445 nm/ RIU, whereas the numerical SRI sensitivity keeps unchanged. It is worth noting that in the range 1.333 (water) to 1.363 (ethanol) the wavelength shift still exhibits a linear behavior where a maximum error of 0.4 nm is measured.

A complete understanding of the difference between numerical and experimental data has not been attained, yet. However, the experimental shift is in very good agreement with resonance shift of the planar 3-D self-assembly structures presented in [5]. They investigated polystyrene nanospheres with diameters of 230 nm, achieving a red shift of 55 nm as SRI moves from air (SRI $=1$) to ethanol (1.363), which is in perfect agreement with the shift obtained here when a

scaling coefficient for the difference in nanospheres size is taken into consideration. In fact, the filling of the air voids with water and then with liquids, i.e., ethanol solutions, of higher refractive index causes a wavelength shift larger than the simulated one. This difference might well be ascribed to a swelling of the PS nanospheres in the presence of the organic solvent [5].

In spite of the simplicity in the fabrication protocols, the achieved SRI sensitivities are significant when compared with alternative fiber probes, including more complex configurations based on metal or metallo-dielectric structures [29], [35], [50]. An SRI sensitivity of 125 nm/ RIU [29] has been demonstrated for a hybrid metallo-dielectric nanostructure fabricated *ad hoc* on a single-mode fiber tip exciting LSPR. Also, Lin *et al*. [29] have obtained an SRI sensitivity of 195.72 nm/ RIU by an ordered array of gold nanodots on a single-mode fiber tip. As well, a very high SRI sensitivity has been recently shown by metal-dielectric crystals fabricated on a fiber tip through a breath figure approach [42].

Fig. 8(b) shows also the theoretical wavelength shift derived by a first order Bragg reflection by [111] planes of the face centered cubic (FCC) structure of the colloidal crystal, thoroughly discussed elsewhere [4], [5], [51], [52]. The resonant wavelength can be expressed as

$$\lambda = \left(\frac{8}{3}\right)^{\frac{1}{2}} 2r\left(\phi n_p + (1-\phi)\, n_m\right) \tag{1}$$

where ϕ is the filling factor, fixed to 0.74 in our geometry, r is the radius of the nanospheres, n_p is the nanospheres refractive index, and n_m the refractive index of the media between the nanospheres.

Evidently, it shows a lower SRI sensitivity as compared to both numerical and experimental data, probability due to the first order approximation. The theoretical shift (vs. air value) is 2.6% and 5.3% lower than the experimental data obtained for water (SRI $=1.333$) and ethanol (SRI $=1.363$), respectively, which is in perfect agreement with the data reported in [5].

Fig. 8(a) also shows a decrease of the reflectance amplitude in and out of the photonic bandgap range with increasing SRI which, in its turn, induces a decrease of the dielectric contrast in the colloidal crystal and a decrease of the discontinuity between the fiber tip and the average external medium, affecting the in- and out-band reflectance respectively.

3. Conclusion

In this work, the fabrication of a photonic bandgap structure consisting of a colloidal crystal self-assembled directly on the surface fiber optics tip has been obtained with a very simple experimental procedure, employing polystyrene nanospheres with 200 nm diameter and UV-VIS optical fibers of 200 μm core. Highly ordered 3-D structures have been produced *via* the immersion of the optical fiber tip in a commercial water suspension of monodisperse PS beads, the effectiveness of the approach being assessed by SEM analysis.

The obtained fiber optic probe exhibits a clear resonant peak in the reflected spectrum which is the signature of the formation of a photonic bandgap structure. Despite the simplicity and the low cost of the fabrication procedure, a good repeatability has been obtained for both the resonant peak wavelength and amplitude. The experimental spectra are in good agreement with numerical studies carried out on a model of the ordered geometry leading to the photonic crystal structure, confirming the production of an ordered assembly on the fiber tip.

The sensing probes proposed here offer valuable sensing features to be exploited in chemical and biological sensing applications. In addition, the possible sensing mechanisms can be widened by considering that the spectral features of the photonic crystals are linked not only to the refractive index of the filling phase, but also to the structural parameters of the lattice (particles size, spacing between the particles, packing geometry) and to the refractive index of the particles themselves. Other spectral features may be added to the optical response by the introduction, among others, of dyes and plasmonic nanoparticles within the colloidal structure, giving rise to more complex sensing probes.

Acknowledgment

The computing resources and the related technical support used for this work have been provided by CRESCO/ENEAGRID High Performance Computing infrastructure and its staff [53]. CRESCO/ENEAGRID High Performance Computing infrastructure is funded by ENEA, the Italian National Agency for New Technologies, Energy and Sustainable Economic Development and by Italian and European research programmes; see http://www.cresco.enea.it/english for information.

References

[1] E. Yablonovitch, "Inhibited spontaneous emission in solid-state physics and electronics," *Phys. Rev. Lett.*, vol. 58, no. 20, pp. 2059–2062, 1987.
[2] S. John, "Strong localization of photons in certain disordered dielectric superlattices," *Phys. Rev. Lett.*, vol. 58, no. 23, pp. 2486–2489, 1987.
[3] J. J. D. Joannopoulos, S. Johnson, J. N. J. Winn, and R. R. D. Meade, *Photonic Crystals: Molding the Flow of Light*. Princeton, NJ, USA: Princeton Univ. Press, 2008.
[4] G. I. N. Waterhouse and M. R. Waterland, "Opal and inverse opal photonic crystals: Fabrication and characterization," *Polyhedron*, vol. 26, no. 2, pp. 356–368, 2007.
[5] S. Kim, Y. G. Seo, Y. Cho, J. Shin, S. C. Gil, and W. Lee, "Optimization of emulsion polymerization for submicron-sized polymer colloids towards tunable synthetic opals," *Bull. Korean Chem. Soc.*, vol. 31, no. 7, pp. 1891–1896, 2010.
[6] A. Blanco *et al.*, "Large-scale synthesis of a silicon photonic crystal with a complete three-dimensional bandgap near 1.5 micrometres," *Nature*, vol. 405, no. 6785, pp. 437–440, 2000.
[7] H. Li *et al.*, "Amplification of fluorescent contrast by photonic crystals in optical storage," *Adv. Mater.*, vol. 22, no. 11, pp. 1237–1241, 2010.
[8] S. Kim, H. Hwang, and S. Yang, "Fabrication of robust optical fibers by controlling film drainage of colloids in capillaries," *Angew. Chem. Int. Ed.*, vol. 51, no. 15, pp. 3601–3605, 2012.
[9] H. S. Lee, T. S. Shim, H. Hwang, S.-M. Yang, and S.-H. Kim, "Colloidal photonic crystals toward structural color palettes for security materials," *Chem. Mater.*, vol. 25, no. 13, pp. 2684–2690, 2013.
[10] K. Ishizaki, K. Suzuki, and S. Noda, "Fabrication of 3D photonic crystals toward arbitrary manipulation of photons in three dimensions," *Photonics*, vol. 3, no. 2, pp. 1–13, 2016.
[11] T. Stomeo *et al.*, "Rapid prototyping of two-dimensional photonic crystal devices by a dual beam focused ion beam system," *Microelectron. Eng.*, vol. 78–79, pp. 417–421, 2005.
[12] G. Rosolen and A. Cola, "Fabrication of photonic crystal structures by electron beam lithography," in *Proc. Conf. Optoelectron. Microelectron. Mater. Devices*, 2006, pp. 66–69.
[13] L. A. Woldering, R. W. Tjerkstra, and W. L. Vos, "Photonic crystal fabrication," *Encyclopedia Mater.: Sci. Technol.*, vol. 7, pp. 1–5, 2011.
[14] O. D. Velev and E. W. Kaler, "Structured porous materials via colloidal crystal templating: From inorganic oxides to metals," *Adv. Mater.*, vol. 12, no. 7, pp. 531–534, 2000.
[15] G. A. Ozin *et al.*, "Nanofabrication by self-assembly," *Mater. Today*, vol. 12, no. 5, pp. 12–23, 2009.
[16] M. Ding, P. Wang, J. Wang, and G. Brambilla, "FIB-milled gold-coated singlemode-multimode-singlemode fiber tip refractometer," *IEEE Photon. Technol. Lett.*, vol. 26, no. 3, pp. 239–241, Feb. 2014.
[17] P. Jiang, J. F. Bertone, K. S. Hwang, and V. L. Colvin, "Single-crystal colloidal multilayers of controlled thickness," *Chem. Mater.*, vol. 11, no. 8, pp. 2132–2140, 1999.
[18] B. Y. Xia, Y. Yin, Y. Lu, and J. Mclellan, "Template-assisted self-assembly of spherical colloids into complex and controllable structures," *Adv. Funct. Mater.*, vol. 13, no. 12, pp. 907–918, 2003.
[19] J. Zhang, Z. Sun, and B. Yang, "Self-assembly of photonic crystals from polymer colloids," *Curr. Opinion Colloid Interface Sci.*, vol. 14, no. 2, pp. 103–114, 2009.
[20] A. Bahrampour *et al.*, "Porphyrin thin films on fiber optic probes through UV-light induced deposition," *Opt. Laser Technol.*, vol. 49, pp. 279–283, 2013.
[21] H. F. Hess *et al.*, "Photonic band gap guidance in optical fibers," *Science*, vol. 282, pp. 1476–1478, 2000.
[22] A. M. R. Pinto and M. Lopez-Amo, "Photonic crystal fibers for sensing applications," *J. Sens.*, vol. 2012, pp. 1–21, 2012.
[23] A. Iadicicco, R. Ranjan, and S. Campopiano, "Fabrication and characterization of long period gratings in hollow core fibers by electric arc discharge," *IEEE Sens. J.*, vol. 15, no. 5, pp. 3014–3020, May 2015.
[24] A. Iadicicco and S. Campopiano, "Sensing features of long period gratings in hollow core fibers," *Sensors*, vol. 15, no. 4, pp. 8009–8019, 2015.
[25] A. Iadicicco, S. Campopiano, and A. Cusano, "Long-period gratings in hollow core fibers by pressure-assisted arc discharge technique," *IEEE Photon. Technol. Lett.*, vol. 23, no. 21, pp. 1567–1569, Nov. 2011.
[26] P. Reader-Harris and A. Di Falco, "Nanoplasmonic filters for hollow core photonic crystal fibers," *ACS Photon.*, vol. 1, no. 10, pp. 985–989, 2014.
[27] T. Zhu, T. Ke, Y. Rao, and K. S. Chiang, "Fabry-Perot optical fiber tip sensor for high temperature measurement," *Opt. Commun.*, vol. 283, no. 19, pp. 3683–3685, 2010.
[28] J. Ma, J. Ju, L. Jin, and W. Jin, "A compact fiber-tip micro-cavity sensor for high-pressure measurement," *IEEE Photon. Technol. Lett.*, vol. 23, no. 21, pp. 1561–1563, Nov. 2011.
[29] M. Consales, A. Ricciardi, A. Crescitelli, E. Esposito, A. Cutolo, and A. Cusano, "Lab-on-fiber technology: Toward multifunctional optical nanoprobes," *ACS Nano*, vol. 6, no. 4, pp. 3163–3170, 2012.

[30] A. Micco, A. Ricciardi, M. Pisco, V. La Ferrara, and A. Cusano, "Optical fiber tip templating using direct focused ion beam milling," *Sci. Rep.*, vol. 5, 2015, Art. no. 15935.
[31] A. Ricciardi *et al.*, "Lab-on-fiber technology: A new vision for chemical and biological sensing," *Analyst*, vol. 140, no. 24, pp. 8068–8079, 2015.
[32] A. Petrušis, J. H. Rector, K. Smith, S. De Man, and D. Iannuzzi, "The align-and-shine technique for series production of photolithography patterns on optical fibres," *J. Micromech. Microeng.*, vol. 19, no. 4, 2009, Art. no. 47001.
[33] H. Yan, M. Wang, Y. Ge, and P. Yu, "Colloidal crystals self-assembled on the end face of fiber: Fabrication and characterizations," *Opt. Fiber Technol.*, vol. 15, no. 3, pp. 324–327, 2009.
[34] Y. Lin, Y. Zou, Y. Mo, J. Guo, and R. G. Lindquist, "E-beam patterned gold nanodot arrays on optical fiber tips for localized surface plasmon resonance biochemical sensing," *Sensors*, vol. 10, no. 10, pp. 9397–9406, 2010.
[35] Y. Lin, Y. Zou, and R. G. Lindquist, "A reflection-based localized surface plasmon resonance fiber-optic probe for biochemical sensing," *Biomed. Opt. Exp.*, vol. 2, no. 3, pp. 478–484, 2011.
[36] A. Dhawan, M. D. Gerhold, and J. F. Muth, "Plasmonic structures based on subwavelength apertures for chemical and biological sensing applications," *IEEE Sens. J.*, vol. 8, no. 6, pp. 942–950, Jun. 2008.
[37] A. Dhawan *et al.*, "Focused ion beam fabrication of metallic nanostructures on end faces of optical fibers for chemical sensing applications," *J. Vac. Sci. Technol. B Microelectron. Nanometer Struct. Process. Meas. Phenom.*, vol. 26, no. 6, pp. 2168–2173, 2008.
[38] M. E. Stewart *et al.*, "Nanostructured plasmonic sensors," *Chem. Rev.*, vol. 108, no. 2, pp. 494–521, 2008.
[39] X. Yang *et al.*, "Nanopillar array on a fiber facet for highly sensitive surface-enhanced Raman scattering," *Opt. Exp.*, vol. 20, no. 22, pp. 24819–24826, 2012.
[40] D. J. White and P. R. Stoddart, "Nanostructured optical fiber with surface-enhanced Raman scattering functionality," *Opt. Lett.*, vol. 30, no. 6, pp. 598–600, 2005.
[41] G. Kostovski, P. R. Stoddart, and A. Mitchell, "The optical fiber tip: An inherently light-coupled microscopic platform for micro- and nanotechnologies," *Adv. Mater.*, vol. 26, no. 23, pp. 3798–3820, 2014.
[42] M. Pisco, F. Galeotti, G. Quero, A. Iadicicco, M. Giordano, and A. Cusano, "Miniaturized sensing probes based on metallic dielectric crystals self-assembled on optical fiber tips," *ACS Photon.*, vol. 1, no. 10, pp. 917–927, 2014.
[43] M. Pisco, G. Quero, A. Iadicicco, M. Giordano, F. Galeotti, and A. Cusano, "Lab on fiber by using the breath figure technique," in *Lab-on-Fiber Technology*, A. Cusano, M. Consales, A. Crescitelli, and A. Ricciardi, Eds., Cham, Switzerland: Springer, 2015, pp. 233–250.
[44] N. Haibin, W. Ming, C. Wei, and W. Tingting, "Assembly photonic crystal arrays on the facet of optical fibers and its applications," in *Proc. Photon. Global Conf.*, 2012, pp. 1–2.
[45] M. Pisco, F. Galeotti, G. Grisci, G. Quero, and A. Cusano, "Self-assembled periodic patterns on the optical fiber tip by microsphere arrays," in *Proc. Int. Conf. Opt. Fibre Sens.*, 2015, p. 96341N–96341N.
[46] A. Ricciardi *et al.*, "Evidence of guided resonances in photonic quasicrystal slabs," *Phys. Rev. B*, vol. 84, no. 8, pp. 1–4, 2011.
[47] S. Fan and J. D. Joannopoulos, "Analysis of guided resonances in photonic crystal slabs," *Phys. Rev. B*, vol. 65, no. 23, pp. 1–8, 2002.
[48] I. H. Malitson, "Interspecimen comparison of the refractive index of fused silica," *J. Opt. Soc. Amer.*, vol. 55, no. 10, pp. 1205–1209, 1965.
[49] N. Sultanova, S. Kasarova, and I. Nikolov, "Dispersion properties of optical polymers," *Acta Phys. Pol. A*, vol. 116, no. 4, pp. 585–587, 2009.
[50] D. Rosenblatt, A. Sharon, and A. A. Friesem, "Resonant grating waveguide structures," *IEEE J. Quantum Electron.*, vol. 33, no. 11, pp. 2038–2059, Nov. 1997.
[51] H. Ding, C. Liu, H. Gu, Y. Zhao, B. Wang, and Z. Gu, "Responsive colloidal crystal for spectrometer grating," *ACS Photon.*, vol. 1, no. 2, pp. 121–126, 2014.
[52] J. Shin, P. V. Braun, and W. Lee, "Fast response photonic crystal pH sensor based on templated photo-polymerized hydrogel inverse opal," *Sens. Actuators, B Chem.*, vol. 150, no. 1, pp. 183–190, 2010.
[53] G. Ponti *et al.*, "The role of medium size facilities in the HPC ecosystem: The case of the new CRESCO4 cluster integrated in the ENEAGRID infrastructure," in *Proc. Int. Conf. High Perform. Comput. Simul.*, 2014, pp. 1030–1033.